






Letter

A full-range formulation for dynamic loss of high-temperature superconductor coated conductors

Hongye Zhang¹ , Hongyi Chen¹, Zhenan Jiang² , Tianhui Yang³ ,
Ying Xin³ , Markus Mueller¹ and Quan Li¹ 

¹ School of Engineering, University of Edinburgh, Edinburgh, EH9 3JL, United Kingdom

² Robinson Research Institute, Victoria University of Wellington, PO Box 33436, Lower Hutt 5046, New Zealand

³ School of Electrical and Information Engineering, Tianjin University, Tianjin 300072, People's Republic of China

E-mail: Hongye.Zhang@ed.ac.uk

Received 6 December 2019, revised 11 February 2020

Accepted for publication 28 February 2020

Published 12 March 2020



Abstract

Dynamic loss is significant for evaluating the performance of type-II high-temperature superconductor (HTS) coated conductors (CC), especially when used in electric machines. Although analytical expressions of dynamic loss have been proposed and verified for HTS CCs exposed to low external magnetic fields with a low current load rate, the non-linearity of dynamic loss at high current load ratios and simultaneous high magnetic fields is still unclear and cannot be predicted by the existing analytical equations. This paper proposes a completely new formulation to characterize the non-linearity of dynamic loss taking into account the $J_c(B)$ dependence of CCs, which can be used for full ranges of both magnetic fields and current load ratios. The proposed analytical formulas have been verified by a T -formulation based numerical model and experiments. This paper comprehensively demonstrates the variation of dynamic loss and provides a meaningful reference of loss controlling for HTS CCs, which is vital for HTS machine windings to avoid quench.

Keywords: dynamic loss, full-range formulation, coated conductor, loss controlling, machine winding

(Some figures may appear in colour only in the online journal)

1. Introduction

Dynamic loss has prompted widespread concern recently in the domains related to second generation (2G) high-temperature superconductor (HTS) coated conductors (CC) [1–5]. It is

generated when HTS CCs carry a direct current (DC) in an alternating current (AC) magnetic field, which is tightly relevant for machine windings and other power applications. The widely adopted analytical expression for dynamic loss per unit time, $Q_{\text{dyn},l}$, can be written as [4]

$$Q_{\text{dyn},l} = 4wfLl_i(B_{\text{ext}} - B_{\text{th}}), \quad (1)$$

where w is the half-width of the HTS CC, f is the frequency of the AC magnetic field, L is the length of the CC, l_i represents the transport current, and i denotes the load ratio between l_i and

Original content from this work may be used under the terms of the [Creative Commons Attribution 4.0 licence](https://creativecommons.org/licenses/by/4.0/). Any further distribution of this work must maintain attribution to the author(s) and the title of the work, journal citation and DOI.

the self-field critical current, I_{c0} . B_{ext} is the amplitude of the external AC magnetic field, and B_{th} is the threshold field, defined by [6]

$$B_{\text{th}} = \frac{\mu_0 h J_{c0}}{2\pi} \left[\frac{1}{i} \ln \left(\frac{1+i}{1-i} \right) + \ln \left(\frac{1-i^2}{4i^2} \right) \right], \quad (2)$$

where μ_0 is the free space permeability, h is the thickness of the HTS thin film, and J_{c0} is the critical current density in self-field, determined by $I_{c0}/(2wh)$.

The linearity of dynamic loss with respect to B_{ext} , as shown in (1), has been well verified by many studies [7–9]. However, recent experimental measurements have shown that, when the HTS CC with a high i is exposed to a high external magnetic field, the dynamic loss exhibits a non-linearity with the augmentation of field intensity and the CC is under the risk of quench [10–12]. A critical-state model for dynamic resistance has been proposed to describe this non-linearity in [8]. When B_{ext} is far greater than B_{th} , dynamic loss can be written as [8]

$$Q_{\text{dyn, nl}} = I_t^2 \cdot \frac{4\omega f L}{I_{c0}} \cdot \left(B_{\text{ext}} + \frac{B_{\text{ext}}^2}{B_0} \right), \quad (3)$$

where B_0 is a constant depending on the material property.

However, it appears that the measured dynamic resistance rises much faster than the analytical results obtained by (3) [8]. Therefore, for now, the existing analytical expressions are inapplicable to characterize the non-linearity of dynamic loss, and the magnetic field and current load ratio causing the sudden rise in loss are still unclear. In [9], a time-averaged DC flux flow resistance has been introduced to explain the non-linear fast rise of dynamic resistance, which provides a good description of the deviation from linearity at high currents. On the basis of this work, we have studied the current density and magnetic flux density distributions inside the HTS CC in detail, and propose a new formulation for dynamic loss, which considers a full-range of magnetic fields and load ratios. This paper helps better understand the variation properties of dynamic loss from the perspective of theoretical fundamentals and determine its influencing factors, which is significant for avoiding quench in HTS machine windings, etc.

2. New formulation of dynamic loss

When a HTS CC carries a DC transport current under an AC magnetic field, the transport current occupies the superconducting layer with width $2iw$ in the center of the CC (named dynamic region), leaving the rest with width $2(1-i)w$ free on both sides [10]. Therefore, the dynamic loss per unit time can be formulated by

$$Q_{\text{dyn}} = \frac{hL}{T} \int_0^T \int_{(1-i)w}^{(1+i)w} E \cdot J dy dt, \quad (4)$$

where E represents the electric field, and J is the current density along the width of the coated conductor.

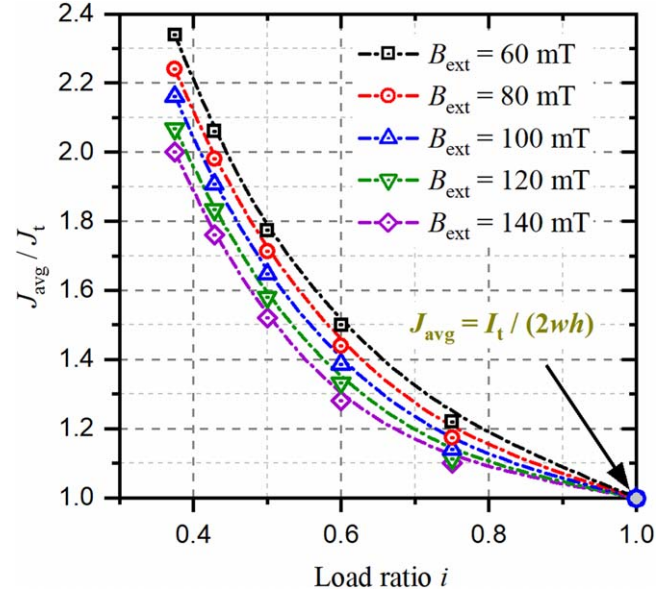


Figure 1. The relationship between J_{avg}/J_t and i under different B_{ext} varying from 60 to 140 mT. Transport current $I_t = 60$ A.

Considering the field dependence of the critical current density $J_c(B)$ [8]

$$J_c(B) = \frac{J_{c0}}{1 + |B_{\perp}|/B_0}, \quad (5)$$

and the E - J power law

$$E = E_0 \cdot \left(\frac{J}{J_c(B)} \right)^n, \quad (6)$$

(4) can be transformed to

$$\begin{aligned} Q_{\text{dyn}} &= \frac{hL}{T} \int_0^T \int_{(1-i)w}^{(1+i)w} E_0 \left[\frac{J \cdot (1 + |B_{\perp}|/B_0)}{J_{c0}} \right]^n J dy dt \\ &= \frac{E_0 h L f}{J_{c0}^n} \int_0^T \int_{(1-i)w}^{(1+i)w} J^{n+1} \cdot f(B) dy dt, \end{aligned} \quad (7)$$

with

$$f(B) = \left[1 + \frac{|B_{\text{ext}} \sin(2\pi f t) - B_s|}{B_0} \right]^n, \quad (8)$$

where $E_0 = 10^{-4} \text{ V m}^{-1}$, B_{\perp} is the local magnetic field perpendicular to the wide surface of the CC. B_{\perp} is decided by both B_{ext} and the self-field B_s . The negative sign indicates the direction of the field vector.

Although the current density and magnetic distribution along the width of the CC has been studied by Brandt, it is not feasible to calculate the integration in (7) directly by analytical methods [13]. However, the non-linear fast rise of dynamic loss occurs when the real load ratio $I_t/I_c(B)$ is approaching 1, i.e., when the CC is in a critical state. In this case, we can simplify (7) by investigating the current density and magnetic flux density characteristics in the dynamic region.

Firstly, the J properties need to be studied. According to the Bean Model, when the superconductor is in a critical state,

the current density distribution along the width of the HTS CC should be characterized by the critical current $\pm J_c$. Here, concerning dynamic loss, we assume that the dynamic region is fully occupied by I_t . To verify this assumption, the T -formulation based numerical modeling method has been adopted here [14, 15]. We define the average current density during one cycle T in the dynamic region, J_{avg} , as

$$J_{\text{avg}} = \frac{1}{T} \cdot \frac{1}{2iw} \cdot \int_0^T \int_{(1-i)w}^{(1+i)w} J dy dt. \quad (9)$$

During the simulation, the transport current I_t has been fixed as 60 A. When I_{c0} decreases from 160 A to 80 A (i.e. i increases from 0.375 to 0.75), the relationship between i and J_{avg}/J_t under different B_{ext} is presented in figure 1. Here, J_t is the average current density determined by the transport current, with $J_t = I_t/(2wh)$. It can be seen that with the increase of i , J_{avg} will get close to J_t . In other words, the dynamic region with the width of $2iw$ is the effective region to carry transport current and in the critical state, the dynamic region has been filled with I_t . Therefore, the current density distribution in the dynamic region should be decided by J_t .

Next, the magnetic flux density properties in the dynamic region need to be explored. In (8), B_s at any position inside the dynamic region, y_0 , is decided by

$$B_s(y_0) = \frac{\mu_0 h}{2\pi} \left[\int_0^{(1-i)w} \frac{J(y)}{(y_0 - y)} dy - \int_{(1-i)w}^{y_0} \frac{J(y)}{(y_0 - y)} dy + \int_{y_0}^{2w} \frac{J(y)}{(y - y_0)} dy \right], \quad (10)$$

Then the average self-field flux density in the dynamic region can be calculated by

$$\begin{aligned} \overline{B_s} &= \frac{1}{2iw} \int_{(1-i)w}^{(1+i)w} B_s(y_0) dy_0 \\ &= \frac{\mu_0 h J_t}{2\pi} \left[\frac{1}{i} \ln \left(\frac{1+i}{1-i} \right) + \ln \left(\frac{1-i^2}{4i^2} \right) \right] = i \cdot B_{\text{th}}. \end{aligned} \quad (12)$$

According to (2), it is evident that B_{th} decreases with i . Therefore, at a high load rate, B_s becomes much smaller compared to B_{ext} , i.e. B_{\perp} will be dominated by the external field. In this case, we have

$$f(B) \approx \left[1 + \frac{|B_{\text{ext}} \sin(2\pi ft)|}{B_0} \right]^n. \quad (13)$$

Based on the above formulas, (7) can be transformed to

$$\begin{aligned} Q_{\text{dyn, nl}} &= \frac{E_0 h L f}{J_{c0}^n} \int_0^T \int_{(1-i)w}^{(1+i)w} \left(\frac{I_t}{2wh} \right)^{n+1} \cdot f(B) dy dt \\ &= \frac{E_0 L f I_t}{2w} i^n \int_0^T \int_{(1-i)w}^{(1+i)w} f(B) dy dt \\ &= E_0 L I_t i^{n+1} \cdot f_{\text{avg}}(B), \end{aligned} \quad (14)$$

with the average of $f(B)$ defined as

$$f_{\text{avg}}(B) = \frac{1}{T} \cdot \frac{1}{2iw} \cdot \int_0^T \int_{(1-i)w}^{(1+i)w} f(B) dy dt, \quad (15)$$

$$Q_{\text{dyn, nl}} = E_0 L I_t i^{n+1} \cdot \left\{ 1 + \sum_{p=0}^{n/2-1} \frac{n!}{(2p+1)![n-(2p+1)]!} \left(\frac{B_{\text{ext}}}{B_0} \right)^{2p+1} \left(\frac{1}{2} \right)^{2p+1} \cdot \frac{2^{3p+2} \cdot p!}{\pi \prod_{q=0}^{2p+1} (2q+1)} \right. \\ \left. + \sum_{p=0}^{n/2-1} \frac{n!}{(2p+2)![n-(2p+2)]!} \left(\frac{B_{\text{ext}}}{B_0} \right)^{2p+2} \left(\frac{1}{2} \right)^{2p+2} \cdot \frac{(2p+2)!}{[(p+1)!]^2} \right\}, \quad (16)$$

$$\begin{aligned} Q_{\text{dyn}} &= Q_{\text{dyn, l}} + Q_{\text{dyn, nl}} = 4w f L I_t i (B_{\text{ext}} - B_{\text{th}}) + E_0 L I_t i^{n+1} \\ &\cdot \left\{ 1 + \sum_{p=0}^{n/2-1} \frac{n!}{(2p+1)![n-(2p+1)]!} \left(\frac{B_{\text{ext}}}{B_0} \right)^{2p+1} \left(\frac{1}{2} \right)^{2p+1} \cdot \frac{2^{3p+2} \cdot p!}{\pi \prod_{q=0}^{2p+1} (2q+1)} \right. \\ &\left. + \sum_{p=0}^{n/2-1} \frac{n!}{(2p+2)![n-(2p+2)]!} \left(\frac{B_{\text{ext}}}{B_0} \right)^{2p+2} \left(\frac{1}{2} \right)^{2p+2} \cdot \frac{(2p+2)!}{[(p+1)!]^2} \right\}. \end{aligned} \quad (17)$$

with $(1-i)w \leq y_0 \leq (1+i)w$.

Based on the above analysis, $J(y)$ is determined by J_t , so (10) can be simplified as

$$B_s(y_0) = \frac{\mu_0 h J_t}{2\pi} \cdot \ln \left(\frac{(2w - y_0) \cdot y_0}{[y_0 - (1-i)w]^2} \right). \quad (11)$$

Based on binomial theorem and Euler's formula, through a series of derivations, the details of which can be found in appendix, (14) can be written as (16). It should be emphasized that $Q_{\text{dyn, nl}}$ in (16) is derived on the basis that the HTS CC is at relatively high i and simultaneous high B_{ext} , which can only be used to characterize the non-linearly fast-rising part of the

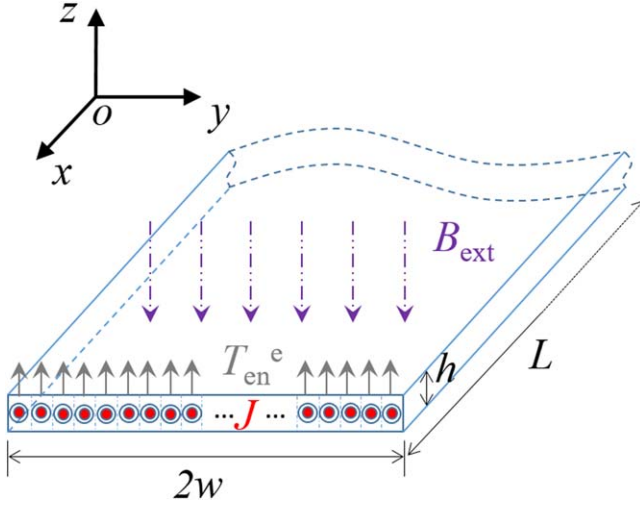


Figure 2. Diagram of the modelling of a HTS CC based on T -formulation by use of finite element method.

$Q_{\text{dyn}}(B_{\text{ext}})$ curve. In (1), $Q_{\text{dyn},l}$ is used to describe the linear correlation between dynamic loss and B_{ext} . There will be a cross point between the $Q_{\text{dyn},l}(B_{\text{ext}})$ and $Q_{\text{dyn},nl}(B_{\text{ext}})$ curves as at low external magnetic field, B_{ext} is much smaller than B_0 , thus the n -value does not play an important role and $Q_{\text{dyn},nl}$ will approach 0. However, at high external field, B_{ext} becomes comparable to B_0 , then under the influence of the n -value, Q_{dyn} will increase rapidly in the form of a power function. In short, before the cross point, $Q_{\text{dyn},l}$ is far greater than $Q_{\text{dyn},nl}$, and vice versa. On the basis of the above analysis, we have proposed a full-range analytical equation for calculating dynamic loss, as (17). It should be noted that, in (17) n is even. When n is odd, we need to modify the upper bound of summation accordingly. To verify the correctness of (17), both numerical modeling and experimental methods have been adopted. In addition, based on the time-averaged DC flux-flow resistance term mentioned in [9], Q_{dyn} can also be fitted by

$$Q_{\text{dyn}} = 4wfLl_t i(B_{\text{ext}} - B_{\text{th}}) + LfI_t^{n+1} \int_0^{1/f} \frac{E_0}{I_c(|B_{\perp}|)^n} dt. \quad (18)$$

(18) has also been compared with (17) in section 4.

3. Validation methods

3.1. Numerical modelling

The numerical model of the HTS CC was developed by use of finite element method based on the T -formulation [14, 15]. The diagram of the modelled HTS CC is shown as figure 2. The governing equation can be written as [4]

$$\frac{1}{\sigma} \nabla^2 T - \frac{\mu_0 h}{2\pi} \cdot \frac{\partial}{\partial t} \sum_{en=1}^{\text{max}} \frac{l_{\text{en}} \nabla \times (T_{\text{en}}^e \mathbf{n}') \cdot \hat{\mathbf{x}}}{r_{\text{en}}} - \frac{\partial \mathbf{B}_{\text{ext}}}{\partial t} \cdot \mathbf{n} = 0, \quad (19)$$

where l_{en} is the width of each element, T_{en}^e is the current vector potential in each element, r_{en} is the distance between

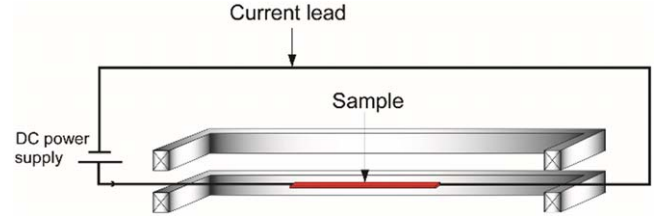


Figure 3. Schematic of the experimental setup to measure the dynamic loss of a HTS CC.

Table 1. Specifications for tested HTS CCS.

Symbols	Parameters	Value	
		Sample 1	Sample 2
w	half width of the CC	2 mm	2 mm
h_{HTS}	YBCO film thickness	1 μm	1 μm
I_{c0}	critical current in self-field	105.3 A	87.67 A
I_t	transport current	95 A	79 A
n	n -value	23	22
f	frequency of the AC field	26.62 Hz	67.89 Hz
B_0	magnetic field constant	0.135 T	0.17 T
T_o	operating temperature	77 K	
E_0	characteristic E -field	10^{-4} V m^{-1}	
μ_0	free space permeability	$4\pi \times 10^{-7} \text{ H m}^{-1}$	

the current source element and the calculation point, \mathbf{n}' is the normal vector at the current source element, \mathbf{n} is the normal vector at the calculation point, and σ is the equivalent conductivity determined by the E - J power law, $\sigma = J/E$.

3.2. Experiment

Two measurement systems were used for the experimental results [3, 9]. One of the experimental setups for measuring Q_{dyn} is shown in figure 3. It is composed of a custom-built AC magnet, which can produce a flux density up to 100 mT, a DC power supply which provides I_t varying between 0–240 A, a nano-voltage meter for averaged voltage measurement across the voltage taps attached on the middle of the sample conductor, and a cryostat containing liquid nitrogen. Q_{dyn} is obtained by multiplying the measured voltage across the sample with the transport current.

Two different YBCO CCs have been tested, of which the specifications are shown in table 1.

4. Results and analyses

For the HTS CCs with different I_{c0} varying from 80 to 160 A while carrying $I_t = 60$ A, they are exposed to AC external magnetic fields with increasing amplitude between 10–500 mT. The simulated Q_{dyn} (solid symbols) and the analytical results calculated by (1) (short dash lines), (16) (dash-dot lines), (17) (solid lines) as well as (18) (dash lines) are depicted together in figure 4.

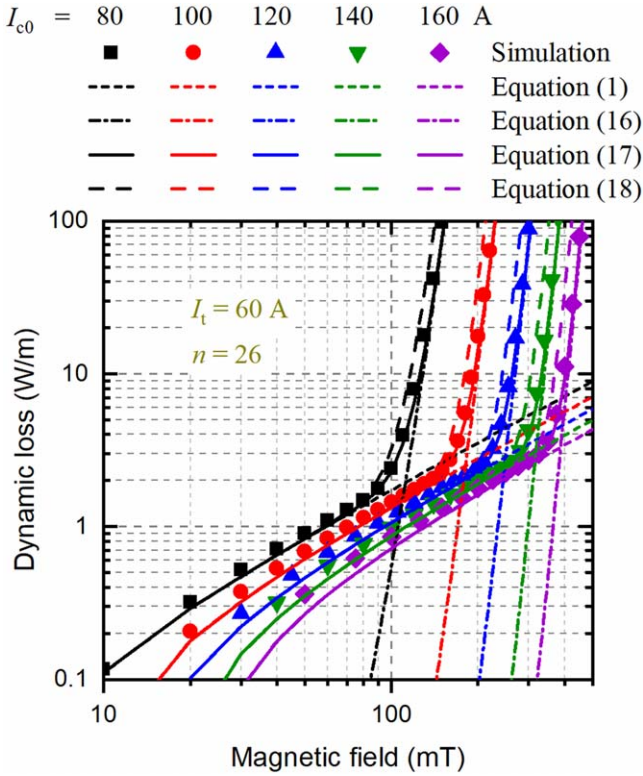


Figure 4. Dynamic loss of HTS CCs with different I_{c0} when changing B_{ext} from 0–500 mT, at 50 Hz.

It shows that there exists a cross-field between the $Q_{dyn,i}(B_{ext})$ and $Q_{dyn,nl}(B_{ext})$ curves, as mentioned above. Before the cross-field, $Q_{dyn}(B_{ext})$ agrees well with (1), which shows a linear correlation. After the cross-field, $Q_{dyn}(B_{ext})$ is in good accordance with (16), which is in the form of a summation of power functions. In general, the simulated $Q_{dyn}(B_{ext})$ agrees well with (17) in the full magnetic field range. Although (18) also describes the non-linearity of Q_{dyn} , it appears to be much larger in terms of value. (17) has been derived through a rigorous process, providing a more accurate result. Furthermore, (18) is given based on the estimation of the time-average DC flux flow resistance, which cannot intuitively account for the non-linearity of Q_{dyn} in the form of a summation of power functions. With regard to the cross-field, it increases inversely with i . In fact, for a lower i the CC has a larger capacity to withstand the induced current by the external magnetic field, thus it will be harder for I_t to go beyond the real critical current $I_c(B)$. Therefore, the cross-field increases with I_{c0} for a fixed I_t , which complies with the $J_c(B)$ dependence and the conclusions drawn in [4].

The simulated Q_{dyn} based on T -formulation, the measured experimental data, and the analytical results obtained by (1), (3), (16) and (17) for the two tested CC samples are presented together in figure 5. It can be found that the experimental data is in good agreement with the simulation results and the proposed equation (17). The $Q_{dyn}(B_{ext})$ curve exhibits an evident non-linearity with the increase of the external magnetic field, which is significantly different from the previously widely-adopted analytical equations (1) and (3). It should be pointed out that the relatively poor agreement between the simulation and experiment at low magnetic fields for the CC sample with

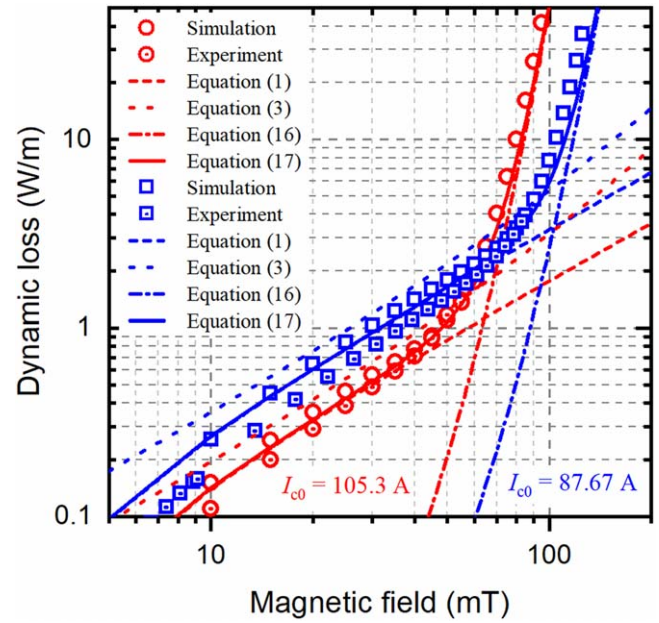


Figure 5. Simulated, measured and analytical dynamic loss of two different HTS CCs. The results in red are for the CC with $I_{c0} = 105.3$ A, and those in blue are for the CC with $I_{c0} = 87.67$ A. According to [3], the effective width of the CC with $I_{c0} = 87.67$ A has been chosen as $2w = 3.51$ mm.

$I_{c0} = 87.67$ A is due to its effective width, which is different from its physical width [3]. However, it does not affect the validity of (17), in that it describes well the non-linearity of Q_{dyn} under high magnetic fields.

With respect to computational complexity, analytical methods generally require far less computing time and resources than the finite element method (FEM) based numerical modelling. In our case, (17) can be simply calculated in a few seconds using MATLAB. However, it requires more time and effort to build and run a FEM model. For example, the computational time to obtain Q_{dyn} of a single HTS layer with the T -formulation based numerical model is tens of seconds or longer, depending on the solving accuracy and number of mesh elements. Therefore, the proposed formulation (17) is a more efficient and convenient way to calculate dynamic loss compared with numerical models.

5. Conclusion

Based on the $J_c(B)$ dependence and E - J power law, through investigation of the characteristics of current density and magnetic flux density distributions in the dynamic region of HTS CCs, a new analytical expression for dynamic loss has been proposed. This expression considers a full-range of magnetic fields and load ratios. At low external fields and simultaneous low load ratios, dynamic loss is in a linear correlation with the external magnetic field. At both high magnetic fields and high load ratios, it is in the form of a summation of power functions. This new formulation can be used to characterize the non-linear variation of dynamic loss, which cannot be accurately predicted and explained by the existing analytical methods. The proposed formulas have been well verified by the T -formulation based numerical modeling method and experiments, which can be achieved in MATLAB

and dramatically save computational effort compared with numerical modelling methods. The cross-field has also been studied, of which the variation complies well with the $J_c(B)$ dependence. This paper comprehensively demonstrates the variation of dynamic loss at different load ratios and magnetic fields. It can serve as a guide for loss controlling and avoiding quench in the application of HTS CCs, especially with regards to machine windings.

Acknowledgments

This work was supported by the joint scholarship from the University of Edinburgh and China Scholarship Council (CSC) under Grant [2018] 3101.

Appendix

According to binomial theorem

$$(a + b)^n = \sum_{k=0}^n \frac{n!}{k!(n-k)!} \cdot a^{n-k} \cdot b^k \quad (\text{A.1})$$

(8) can be expanded into

$$\begin{aligned} f(B) &= \left[1 + \frac{|B_{\text{ext}} \sin(2\pi ft)|}{B_0} \right]^n = 1 + n \frac{|B_{\text{ext}} \sin(2\pi ft)|}{B_0} \\ &+ \frac{n(n-1)}{2!} \left(\frac{|B_{\text{ext}} \sin(2\pi ft)|}{B_0} \right)^2 \\ &+ \frac{n(n-1)(n-2)}{3!} \left(\frac{|B_{\text{ext}} \sin(2\pi ft)|}{B_0} \right)^3 + \dots \end{aligned} \quad (\text{A.2})$$

According to Euler's formula

$$e^{ix} = \cos x + i \sin x \quad (\text{A.3})$$

we have

$$\begin{aligned} \sin^N x &= \left[\frac{1}{2i} (e^{ix} - e^{-ix}) \right]^N \\ &= \left(\frac{1}{2i} \right)^N \cdot \sum_{k=0}^N \frac{N!}{k!(N-k)!} (e^{ix})^{N-k} (-e^{-ix})^k \\ &= \left(\frac{1}{2i} \right)^N \cdot \sum_{k=0}^N \frac{N!}{k!(N-k)!} (-1)^k \\ &\times \left\{ \cos[(N-2k)x] + i \sin[(N-2k)x] \right\}. \end{aligned} \quad (\text{A.4})$$

When N is odd, we have

$$|\sin^N x| = \left(\frac{1}{2} \right)^N \left| \sum_{k=0}^N \frac{N!}{k!(N-k)!} (-1)^k \sin[(N-2k)x] \right|. \quad (\text{A.5})$$

On the contrary, when N is even we get

$$|\sin^N x| = \left(\frac{1}{2} \right)^N \left| \sum_{k=0}^N \frac{N!}{k!(N-k)!} (-1)^k \cos[(N-2k)x] \right|. \quad (\text{A.6})$$

Based on (A.1)–(A.6), (15) can be expanded to

$$\begin{aligned} f_{\text{avg}}(B) &= \frac{1}{T} \cdot \frac{1}{2i\omega} \cdot \int_0^T \int_{(1-i)\omega}^{(1+i)\omega} f(B) dy dt \\ &= \frac{1}{T} \cdot \frac{1}{2i\omega} \cdot \int_0^T \int_{(1-i)\omega}^{(1+i)\omega} \left[1 + \frac{|B_{\text{ext}} \sin(2\pi ft)|}{B_0} \right]^n dy dt \\ &= \sum_{k=0}^n \frac{n!}{k!(n-k)!} \left(\frac{B_{\text{ext}}}{B_0} \right)^k \cdot \frac{1}{T} \int_0^T |\sin^k(2\pi ft)| dt \\ &= \sum_{k=0}^n \frac{n!}{k!(n-k)!} \left(\frac{B_{\text{ext}}}{B_0} \right)^k \cdot \frac{1}{T} \int_0^T \left| \left(\frac{1}{2i} \right)^k \cdot \sum_{m=0}^k \frac{k!}{m!(k-m)!} (-1)^m \left\{ \cos[2\pi(k-2m)ft] + i \sin[2\pi(k-2m)ft] \right\} \right| dt \\ &= \sum_{p=0}^{n/2-1} \frac{n!}{(2p+1)![n-(2p+1)]!} \left(\frac{B_{\text{ext}}}{B_0} \right)^{2p+1} \left(\frac{1}{2} \right)^{2p+1} \cdot \frac{1}{T} \int_0^T \left| \sum_{m=0}^{2p+1} \frac{(2p+1)!}{m!(2p+1-m)!} (-1)^m \sin[2\pi(2p+1-2m)ft] \right| dt \\ &+ \sum_{p=0}^{n/2-1} \frac{n!}{(2p+2)![n-(2p+2)]!} \left(\frac{B_{\text{ext}}}{B_0} \right)^{2p+2} \left(\frac{1}{2} \right)^{2p+2} \cdot \frac{1}{T} \int_0^T \left| \sum_{m=0}^{2p+2} \frac{(2p+2)!}{m!(2p+2-m)!} (-1)^m \cos[2\pi(2p+2-2m)ft] \right| dt \\ &= 1 + \sum_{p=0}^{n/2-1} \left\{ \frac{n!}{(2p+1)![n-(2p+1)]!} \left(\frac{B_{\text{ext}}}{B_0} \right)^{2p+1} \frac{2^{p+1} \cdot p!}{\pi \prod_{q=0}^{2p+1} (2q+1)} + \frac{n!}{(2p+2)![n-(2p+2)]!} \left(\frac{B_{\text{ext}}}{B_0} \right)^{2p+2} \frac{(2p+2)!}{2^{2p+2} \cdot [(p+1)!]^2} \right\}. \end{aligned} \quad (\text{A.7})$$

Therefore, (14) can be written as

$$Q_{\text{dyn, nl}} = E_0 L l i^{n+1} \cdot f_{\text{avg}}(B) = E_0 L l i^{n+1} \cdot \left\{ 1 + \sum_{p=0}^{n/2-1} \frac{n!}{(2p+1)![n-(2p+1)]!} \left(\frac{B_{\text{ext}}}{B_0} \right)^{2p+1} \left(\frac{1}{2} \right)^{2p+1} \cdot \frac{2^{3p+2} \cdot p!}{\pi \prod_{q=0}^{2p+1} (2q+1)} + \sum_{p=0}^{n/2-1} \frac{n!}{(2p+2)![n-(2p+2)]!} \left(\frac{B_{\text{ext}}}{B_0} \right)^{2p+2} \left(\frac{1}{2} \right)^{2p+2} \cdot \frac{(2p+2)!}{[(p+1)!]^2} \right\}. \quad (\text{A.8})$$

ORCID iDs

Hongye Zhang  <https://orcid.org/0000-0002-8960-4614>

Zhenan Jiang  <https://orcid.org/0000-0002-3482-3510>

Tianhui Yang  <https://orcid.org/0000-0002-8481-0187>

Ying Xin  <https://orcid.org/0000-0001-7835-3832>

Quan Li  <https://orcid.org/0000-0001-7153-0656>

References

- [1] Jiang Z *et al* 2014 Dynamic resistance of a high- T_c superconducting flux pump *Appl. Phys. Lett.* **105** 112601
- [2] Ainslie M D *et al* 2018 Numerical modelling of dynamic resistance in high-temperature superconducting coated-conductor wires *Supercond. Sci. Technol.* **31** 1–16
- [3] Jiang Z *et al* 2018 The dynamic resistance of YBCO coated conductor wire: effect of DC current magnitude and applied field orientation *Supercond. Sci. Technol.* **31** 035002
- [4] Zhang H *et al* 2019 Dependence of dynamic loss on critical current and n -value of HTS coated conductors *IEEE Trans. Appl. Supercond.* **29** 1–7
- [5] Ciszek M *et al* 2002 Angular dependence of the dynamic resistance and its relation to the AC transport current loss in Bi-2223/Ag tape superconductors *Supercond. Sci. Technol.* **15** 1275–80
- [6] Mikitik G *et al* 2001 Generation of a dc voltage by an ac magnetic field in type-II superconductors *Phys. Rev. B* **64** 092502
- [7] Matsushita T 1994 *Flux Pinning and Electromagnetic Phenomenon*. (Tokyo, Japan: Sangyo Tosho, Inc) pp 99
- [8] Oomen M P *et al* 1999 Dynamic resistance in a slab-like superconductor with $J_c(B)$ dependence *Supercond. Sci. Technol.* **12** 382–7
- [9] Jiang Z *et al* 2017 Dynamic resistance of a high- T_c coated conductor wire in a perpendicular magnetic field at 77 K *Supercond. Sci. Technol.* **30** 03LT01
- [10] Li Q *et al* 2018 Numerical modeling of dynamic loss in HTS-coated conductors under perpendicular magnetic fields *IEEE Trans. Appl. Supercond.* **28** 1–6
- [11] Jiang Z *et al* 2017 Dynamic resistance measurements in a GdBCO-Coated conductor *IEEE Trans. Appl. Supercond.* **27** 1–5
- [12] Jiang Z *et al* 2018 Dynamic resistance measurement of a four-tape YBCO stack in a perpendicular magnetic field *IEEE Trans. Appl. Supercond.* **28** 1–5
- [13] Brandt E H *et al* 1993 Type-II super-conductor strip with current in a perpendicular magnetic field *Phys. Rev. B* **48** 12893–906
- [14] Levin G A *et al* 2005 Magnetization losses in multiply connected $\text{YBa}_2\text{Cu}_3\text{O}_{6+x}$ -coated conductors *J. Appl. Phys.* **98** 113909
- [15] Amemiya N *et al* 2006 Magnetic flux penetration into twisted multifilamentary coated superconductors subjected to ac transverse magnetic fields *J. Appl. Phys.* **100** 123907